A Novel Image Inpainting Technique Based on Isotropic Diffusion

Zainab A. Abdul Kareem[1,*], Ahmed K. Al-Jaberi[2]

1. Department of Mathematics, College of Science, University of Basrah, Basra, Iraq.

2. Department of Mathematics, College of Education for Pure Science, University of Basrah, Basra, Iraq.

*Corresponding author: E-mail: zayanb.eali.sci@uobasrah.edu.iq

Doi:10.29072/basjs.20220203

ARTICLE INFO

Keywords

Image inpainting. isotropic equation. PDE-based inpainting method. Image quality assessments.

.

ABSTRACT

Using the isotropic diffusion model as a foundation, a novel method for image inpainting was suggested. To restore various missing areas of diverse natural images, a modified version of the original isotropic model is used. When employing the original isotropic model, the results of the suggested technique are compared to those obtained results. Regarding building texture in the missing area and restoring significant missing sections, the results of the suggested model performed better than the results of the obtained isotropic model. The performance of the suggested model in comparison to the original isotropic model is examined using a number of picture quality measures, including MSE, PSNR, and SSIM. In comparation to the widely used isotropic model, the improved model performs better and provides better measures of quality assessment for a greater number of natural photos.

Received 11 Jun 2022; Received in revised form 13 July 2022; Accepted 10 Aug 2022, Published 31 Aug 2022

This article is an open access article distributed under the terms and conditions of the Creative Commons Attribution-NonCommercial 4.0 International (CC BY-NC 4.0 license) (http://creativecommons.org/licenses/by-nc/4.0/).

1. Introduction

Image inpainting is a process that aims to restore the damaged part in the image to reconstruct it and generate a high-quality semantic approximation to the original image [1]. Image inpainting was created in art, inpainting of degraded painting was done by professional artists while in mathematics, inpainting refers to filling in the damaged regions by the propagation of available information from their surroundings areas in the image [2]. Improving the quality of damaged and noisy images is a fundamental task in image processing to make the recognition process as easy and automatic as possible. Thus, image inpainting became an important subject of research with wide fields of applications such as medical imaging, augmented reality, art, computer-assisted restoration, image coding [3], and transmission [4], as well as virtual restoration of digitized paintings [5, 6]. Inpainting algorithms could be classified into three main approaches diffusion-based, exemplar-based [7], and machine learning-based ways [7]. Masnou and Morel firstly proposed the diffusion-based approach where the level lines-based disocclusion yields a result that has strong discontinuities [8]. Bertalmio et al. solved the inpainting process using diffusion partial differential equation (PDE) where the boundary information propagates into the region to be inpainted along the direction of isophotes [9]. PDE-based methods are both theoretically and computationally sound as they are based on and backed by the theory of PDEs and numerical analysis. Therefore, PDEs methods led to suggest a new model for solving inpainting problems with a cost-effective method of solution [10]. However, the PDE approaches have two forms are linear (isotropic) [11] and non-linear (anisotropic) [12], where the linear models are the oldest and simplest ones that used to restore the missing area in the images. Although, the liner models appear strong smoothing effect on the missing area but destroy important features of the image like the edge that appears blurred especially in the case of a large missing area. Thus, many nonlinear models are suggested to solve this problem by slowing down the diffusion near the edges [13]. Although isotropic models fail to restore the edges of the images and give an image identical to the original image, but it is a successful model for removing noise. An accurate evaluation method that simultaneously estimate inpainted images is not an easy and not fully solved yet [14]. Therefore, visual analysis is take to assess the quality of inpainted images while the quantitative evaluation was determined through statistical measurements to estimate the quality of the inpainted images. Mean Squared Error (MSE), Structural Similarity (SSIM) and Peak Signal-to-Noise Ratio (PSNR) [10, 15] are used to estimate the quality of the inpainted image by the original and modified isotropic model. In the present work, the isotropic model-based inpainting has been modified and the obtained results are enhanced compared to the original

This article is an open access article distributed under the terms and conditions of the Creative Commons Attribution-NonCommercial 4.0 International (CC BY-NC 4.0 license) (http://creativecommons.org/licenses/by-nc/4.0/).

isotropic model. In the present work, a new technique for inpainting images based on isoptrobic model has been suggested and tested. Further, the numerical solution of the modified model was studied.

2. Isotropic Diffusion Model

Diffusion-based inpainting is the first model was used to recover the damaged or missing part of the image by spreading information from the surrounding area of the missing region at the pixel point [16, 17]. However, the isotropic diffusion is the second order linear parabolic equation. Let $f \in L^2(\Omega)$ is an image and $D \subset \Omega$ is a missing information region from the original image; u is the inpainted image given by the solution of the below equation [18]:

$$\begin{cases} u_t = \Delta u, & t \geq 0 \\ u(0,x,y) = 0. \end{cases} \qquad 1$$

In addition, u can be calculated from the solution of minimization functional for the squared total variation. Heat equation was introduced as minimization energy functional as [19]:

$$\min_{u \in L^2(\Omega)} \{ \iint |\nabla u|^2 \, dxdy \quad such\ that \quad u = f \ in\ \Omega \backslash D \} \qquad 2$$

Euler- Lagrange equation and gradient descent method are applied on the minimization functional 2, we get

$$u_t = \Delta u \qquad 3$$

The solution of equation 1 or 3 with the Dirichlet boundary condition is used to recover the missing regions in the image. The explicit finite difference method (EFEM) applied to find the solution of equation 1 or 3, which is imitative the solution of the heat equation on the spatial (image) domain. This equation is studied the spreading of temperatures (information) within a period in all directions based on the boundary condition [17]. However, the spread in all directions will cause failure to recover edge construction of the missing area and appear blurred under the isotropic model. The diffusion term comes from the idea of propagating local information with smoothness constraints by analogy with some physical phenomena like heat propagation in physical structures [8]. Isotropic diffusion acts as low-pass linear filtering suppressing high frequencies in the image thus, it works to minimize these variations in all directions that in turn led to appearing blurred close to edges and contours. More general formalisms using nonlinear PDEs are used for describing the physical and fluid dynamics phenomena to get better restoration of edges and more sharpness [9].

This article is an open access article distributed under the terms and conditions of the Creative Commons Attribution-NonCommercial 4.0 International (CC BY-NC 4.0 license) (http://creativecommons.org/licenses/by-nc/4.0/).

3. Modify The Isotropic Diffusion Model

The isotropic diffusion model is modified by adding more than one algebraic expression to reduce the blurry of the large missing area and enhance the edge of restoration. Modified isotropic model is proposed by adding the first derivative of the missing area of the image. The ability of the first derivative helps to build the edges and extend the isophote line, which improves of recovering missing areas. The modified isotropic equation writes as follows:

$$u_t = \Delta u + \alpha u_x + \beta u_y , \quad t \geq 0 \qquad 4$$

Where u_x and u_y are first derivatives of image, the α and β are coefficients. Furthermore, the value of α and β play an important effect on the values of quality measures. The numerical solutions of modified isotropic diffusion model give in next section.

3.1. Numerical Solution Of The Modified Isotropic Equation

The EFDM is used to find the numerical solution of the modified equation with Dirichlet boundary conditions. A dopt the notation

$$U = u(x, y, t) = u(i\Delta x, j\,\Delta y\,, n\Delta t\,) = u_{i,j}^{n} \qquad 5$$

The derivative formula becomes:

$$u_x(i\Delta x, j\,\Delta y\,, n\Delta t\,) = \frac{\partial u(i\Delta x, j\,\Delta y\,, n\Delta t\,)}{\partial x} = \frac{u_{i+1,j}^{n} - u_{i-1,j}^{n}}{2\Delta x} \qquad 6$$

$$u_y(i\Delta x, j\,\Delta y\,, n\Delta t\,) = \frac{\partial u(i\Delta x, j\,\Delta y\,, n\Delta t\,)}{\partial y} = \frac{u_{i,j+1}^{n} - u_{i,j-1}^{n}}{2\Delta y} \qquad 7$$

The modified isotropic equation formula is given by:

$$U_t = U_{xx} + U_{yy} + \alpha U_x + \beta U_y \qquad 8$$

The modified isotropic equation in eq.8 is rewritten using the EFDM:

$$u_{i,j}^{n+1} = \frac{\Delta t}{\Delta x^2}\left[u_{i+1.j}^{n} - 2u_{i,j}^{n} + u_{i-1,j}^{n}\right] + \frac{\Delta t}{\Delta y^2}\left[\, u_{i,j+1}^{n} - 2u_{i,j}^{n} + u_{i,j-1}^{n} \,\right] +$$

$$u_{i,j}^{n} + \alpha\Delta t\left(\frac{u_{i+1,j}^{n} - u_{i-1,j}^{n}}{2\Delta x}\right) + \beta\Delta t\left(\frac{u_{i,j+1}^{n} - u_{i,j-1}^{n}}{2\Delta y}\right)$$

9

Where $\Delta x = \Delta y = h = 1$. Let $\frac{\Delta t}{h^2} = r$, Δt = 0.005.Thus, the equation 9 will be:

$$u_{i,j}^{n+1} = ru_{i+1.j}^{n} - 4ru_{i,j}^{n} + ru_{i-1,j}^{n} + ru_{i,j+1}^{n} + ru_{i,j-1}^{n} + u_{i,j}^{n} + \frac{\alpha\Delta t}{2}\left(u_{i+1,j}^{n} - u_{i-1,j}^{n}\right) +$$

$$\frac{\beta\Delta t}{2}\left(u_{i,j+1}^{n} - u_{i,j-1}^{n}\right) \qquad 10$$

This article is an open access article distributed under the terms and conditions of the Creative Commons Attribution-NonCommercial 4.0 International (CC BY-NC 4.0 license) (http://creativecommons.org/licenses/by-nc/4.0/).

However, eq. 10 can be simplified to be equation 11:

$$u_{i,j}^{n+1} = (1-4r)u_{i,j}^{n} + (r+\frac{\alpha\Delta t}{2})u_{i+1.j}^{n} + (r-\frac{\alpha\Delta t}{2})u_{i-1,j}^{n} + (r+\frac{\beta\Delta t}{2})u_{i,j+1}^{n} + (r-\frac{\beta\Delta t}{2})u_{i,j-1}^{n} \quad 11$$

The stability of the modified model is studied using different values of α and β and found that the model will be stable when: $0 \le \alpha \le 1$, $0 \le \beta \le 1$, and $\alpha + \beta \le 1$. Three cases of α and β values are selected to test the modified model depending on the texture direction. When the texture direction is horizontally extended, the values of α=0 and β=1 while α=1 and β=0 are selected for the vertically extended texture direction. However, for diagonal texture, the $\alpha, \beta \in (0,1)$; $\alpha + \beta < 1$. Thus, the third case for diagonal texture was studied using $\alpha = \beta = 1/2$. Figure1 shows an image containing vertical twigs that are inpainted using three suggested values of $\alpha = \beta = 1/2$ in Figure1c, $\alpha = 1$ and $\beta = 0$ in Figure1d, and $\alpha = 0$, and $\beta = 1$ in Figure1e. When $\alpha = \beta = 1/2$ are selected, the twigs in the inpainted image appeared slant due to the two derivatives existing in the modified model and have the same effect on the direction of the derivative. However, when $\alpha = 1$ and $\beta = 0$, the restoration of twigs in the inpainted image was good because the texture was in the same direction with derivative diffusion (u_x) while when $\alpha = 0$ and $\beta = 1$, the restoration of twigs is failed due to the direction of texture was reversed the direction derivative diffusion (u_y).

Figure1: Effect of α and β values on image inpainting, (a) original image, (b) masked image, (c) inpainted image with α=β=1/2, (d) inpainted image with α=1, β=0, and (e) inpainted image with α=0, β=1

3.2. Stability Of Modify Isotropic Model

Numerical stability problems related to some finite difference (FD)approximations of two _dimensional modify isotropic model. The isotropic equation formula given by:

This article is an open access article distributed under the terms and conditions of the Creative Commons Attribution-NonCommercial 4.0 International (CC BY-NC 4.0 license) (http://creativecommons.org/licenses/by-nc/4.0/).

$$u_t = K(u_{xx} + u_{yy}) \quad 12$$

modify isotropic model when k>0:

$$u_t = K(u_{xx} + u_{yy}) + \alpha u_x + \beta u_y \quad 13$$

An explicit finite difference representation of the equation (13) can be obtained by a forward time center space differencing

$$\frac{u_{i,j}^{n+1}-u_{i,j}^{n}}{\Delta t} = k\left(\frac{u_{i+1,j}^{n}-2u_{i,j}^{n}+u_{i-1,j}^{n}}{\Delta x^2} + \frac{u_{i,j+1}^{n}-2u_{i,j}^{n}+u_{i,j-1}^{n}}{\Delta y^2}\right) + \alpha\left(\frac{u_{i+1,j}^{n}-u_{i-1,j}^{n}}{2\Delta x}\right) + \beta\left(\frac{u_{i,j+1}^{n}-u_{i,j-1}^{n}}{2\Delta y}\right) \quad 14$$

By Von Neumann's method

$$E_{p,o,q} = e^{i\vartheta(ph)}.e^{i\gamma(os)}.\varepsilon^{q} \quad 15$$

where $E_{p,o,q}$ *is error*

$$u(x,y,t_n) = e^{i(\vartheta,\gamma)\binom{x}{y}} = e^{i\vartheta x}.e^{i\gamma y} \quad 16$$

Let $x=ph$,$y=os$. Now substitute in the equation (14):

$$e^{i\vartheta(ph)}.e^{i\gamma(os)}.\varepsilon^{q+1} - e^{i\vartheta(ph)}.e^{i\gamma(os)}.\varepsilon^{q} = K\left(\frac{e^{i\vartheta(p+1)h}.e^{i\gamma(os)}.\varepsilon^{q}-2e^{i\vartheta(ph)}.e^{i\gamma(os)}.\varepsilon^{q}+e^{i\vartheta(p-1)h}.e^{i\gamma(os)}.\varepsilon^{q}}{\Delta x^2}\right) + \frac{e^{i\vartheta(ph)}.e^{i\gamma(o+1)s}.\varepsilon^{q}-2e^{i\vartheta(ph)}.e^{i\gamma(os)}.\varepsilon^{q}+e^{i\vartheta(ph)}.e^{i\gamma(o-1)s}.\varepsilon^{q}}{\Delta y^2}) + \alpha\left(\frac{e^{i\vartheta(p+1)h}.e^{i\gamma(os)}.\varepsilon^{q}-e^{i\vartheta(p-1)h}.e^{i\gamma(os)}.\varepsilon^{q}}{2\Delta x}\right) + \beta\left(\frac{e^{i\vartheta(ph)}.e^{i\gamma(o+1)s}.\varepsilon^{q}-e^{i\vartheta(ph)}.e^{i\gamma(o-1)s}.\varepsilon^{q}}{2\Delta y}\right) \quad 17$$

Divide equation 17 by $(e^{i\vartheta(ph)}.e^{i\gamma(os)}.\varepsilon^{q})$ leads to the equation 18:

$$\frac{\varepsilon-1}{\Delta t} = K\left(\frac{e^{i\vartheta h}-2+e^{-i\vartheta h}}{\Delta x^2} + \frac{e^{i\gamma s}-2+e^{-i\gamma s}}{\Delta y^2}\right) + \alpha\left(\frac{e^{i\vartheta h}-e^{-i\vartheta h}}{2\Delta x}\right) + \beta\left(\frac{e^{i\gamma s}-e^{-i\gamma s}}{2\Delta y}\right) \quad 18$$

In a simpler form, we consider $\alpha = \beta$

$$\varepsilon - 1 = \frac{\Delta tK}{\Delta x^2}(2cos\vartheta h - 2) + \frac{\Delta tk}{\Delta y^2}(2cos\gamma s - 2) + \alpha\frac{\Delta t}{\Delta x}isin\,\vartheta h + \alpha\frac{\Delta t}{\Delta y}isin\,\gamma s, \quad 19$$

Where $r_x = \frac{\Delta tK}{\Delta x^2}$, $r_y = \frac{\Delta tK}{\Delta y^2}$, $\Delta x = \Delta y = 1$ then $r_x = r_y = r$

This article is an open access article distributed under the terms and conditions of the Creative Commons Attribution-NonCommercial 4.0 International (CC BY-NC 4.0 license) (http://creativecommons.org/licenses/by-nc/4.0/).

and let $\mu_y = \alpha\frac{\Delta t}{\Delta y} \leq 1$ is Courant Fried Richs Lewy (CFL) condition[20]. Where μ_y *is called CFL* number. In general the explicit finite difference methods will require that the CFL be bonded by a constant which will depend upon the particular numerical scheme $\mu = \mu_x = \mu_y$ Now substitute in the equation (19):

$$\varepsilon - 1 = 2r(\cos\vartheta h - 1) + 2r(\cos\gamma s - 1) + \mu i \sin\gamma s + \mu i \sin\vartheta h \quad 20$$

This gives a complex amplification factor, the modulus of which reads

$$\varepsilon\bar{\varepsilon} = |\varepsilon|^2 = \left(1 - 4r\left(sin^2\frac{\vartheta h}{2} + sin^2\frac{\gamma s}{2}\right)\right)^2 - \mu^2\left(\frac{\sin\gamma s}{2} + \frac{\sin\vartheta h}{2}\right)^2 \quad 21$$

Hence $r \leq 1/4,\ \mu \leq 1$ [21]. by Van Neumann stability condition $|\varepsilon|^2 \leq 1$:

$$(1 - 4r\left(sin^2\frac{\vartheta h}{2} + sin^2\frac{\gamma s}{2}\right))^2 - \mu^2(sin\frac{\gamma s}{2} + sin\frac{\vartheta h}{2})^2 \leq 1 \quad 22$$

Either

$$(1 - 4r\left(sin^2\frac{\vartheta h}{2} + sin^2\frac{\gamma s}{2}\right)) - \mu(sin\frac{\gamma s}{2} + sin\frac{\vartheta h}{2}) \leq 1 \quad 23$$

$$-\mu \leq \frac{4r(sin^2\frac{\vartheta h}{2} + sin^2\frac{\gamma s}{2})}{sin\frac{\gamma s}{2} + sin\frac{\vartheta h}{2}} \quad 24$$

$$\frac{4r\left(sin^2\frac{\vartheta h}{2} + sin^2\frac{\gamma s}{2}\right)}{\frac{\sin\gamma s}{2} + \frac{\sin\vartheta h}{2}} \approx 1 \quad 25$$

That lead to $\mu > -1,$ 26

or when : $(1 - 4r\left(sin^2\frac{\vartheta h}{2} + sin^2\frac{\gamma s}{2}\right)) + \mu(sin\frac{\gamma s}{2} + sin\frac{\vartheta h}{2}) \leq 1$ 27

$$\mu \leq \frac{4r(sin^2\frac{\vartheta h}{2} + sin^2\frac{\gamma s}{2})}{sin\frac{\gamma s}{2} + sin\frac{\vartheta h}{2}} \quad 28$$

That lead to $\mu \leq 1$ 29

From the equations (26) and (29) get :

This article is an open access article distributed under the terms and conditions of the Creative Commons Attribution-NonCommercial 4.0 International (CC BY-NC 4.0 license) (http://creativecommons.org/licenses/by-nc/4.0/).

$$-1 < \mu \leq 1 \qquad 30$$

By CFL condition has the following properties If $\mu = \alpha \frac{\Delta t}{\Delta y} \leq 1$ in 1- dim. Then,

$\mu = \mu_y + \mu_x \leq 1$ in 2-dim.

i.e $$\alpha_x \frac{\Delta t}{\Delta x} + \alpha_y \frac{\Delta t}{\Delta y} \leq 1 \qquad 31$$

suppose that $\alpha=\alpha_x = \alpha_y$ and $\Delta x=\Delta y$ .Then the equation (31) is become as:

$$2\alpha \frac{\Delta t}{\Delta x} \leq 1 \qquad 32$$

And that leads to $2\,\mu \leq 1$ and $\mu \leq \frac{1}{2}$ when $|\alpha|> 0$.

4. Experimental Results

The suggested modification of the isotropic model was tested on a different 20 natural images chased from Berkeley Segmentation Dataset and Benchmarks 300 (BSDS300) [21]. The results of the proposed technique are compared with those obtained using the original isotropic technique. The chosen images have various sizes of the missing area to test the effectiveness of the proposed modified model for the restoration of the missing area. Further, to find out the ability and effectiveness of the suggested model through filling the gaps, virtual masks are used to make gaps in the image. Four types of masks are square, narrow rectangular, and large rectangular shapes in the different sizes and locations of the image. The Matlab programming was used to test the proposed model on the selected standard natural images. Figure 2 shows a group of images selected to test the effect of α and β values on the inpainted images. When $\alpha = \beta = 1/2$,the twigs has been restored perfectly in image in the first and second cases while when α≠ β, the twigs was not good restored with unclear edges. Furthermore, in the third case, the best results was obtained when the value α=0 and β=1where the beach boundaries were restored in the image. Finally, the best inpainted image when α=0 and β=1 compared to other α and β values in the fourth case

This article is an open access article distributed under the terms and conditions of the Creative Commons Attribution-NonCommercial 4.0 International (CC BY-NC 4.0 license) (http://creativecommons.org/licenses/by-nc/4.0/).

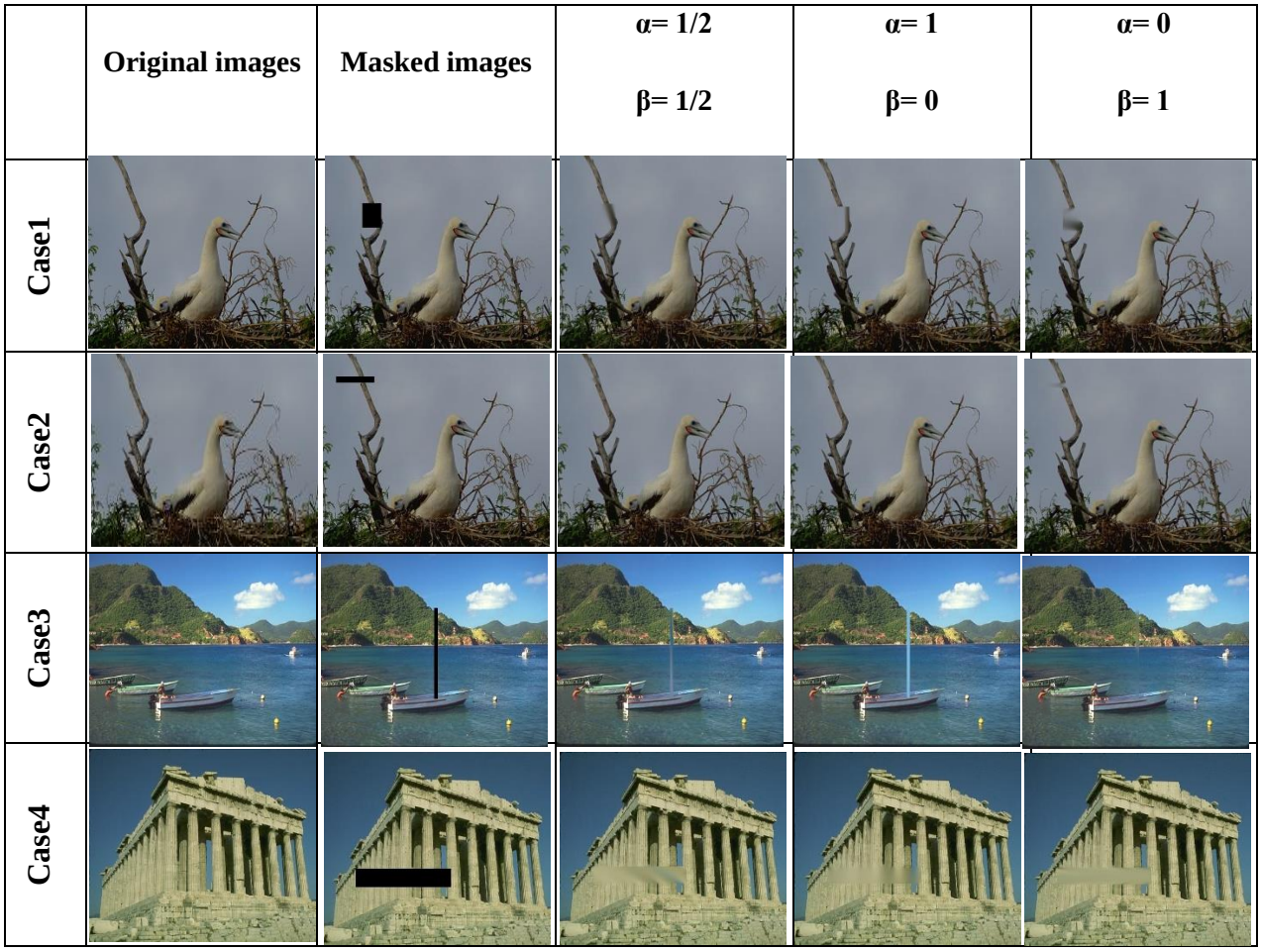

Figure2: Effect of α and β values onto the inpainted images using different types of mask.

4.1 Image Quality Assessment

Three different statistical quality measurements will be used to assess the quality of inpainted images, and the performance of the proposed model. These quality measures can be estimated the quality between the original and inpainted images. Firstly, the mean square error (MSE) will apply to find the difference between the inpainted image I' and the original image I given by [10]:

$$MSE = \frac{1}{(NMR)} \sum_{q=1}^{Q} \sum_{n=1}^{N} \sum_{m=1}^{M} [\, I_q(n,m) - I'_q(n,m) \,]^2 \quad , \qquad 33$$

where q is the number of channels in a color image, n is the number of rows and m is the number of columns in the channel. Secondly, the other measure is the peak signal to noise ratio (PSNR) which can be found in [10]:

$$PSNR = 10 \log_{10}\left(\frac{255^2}{MSE}\right) \qquad 34$$

This article is an open access article distributed under the terms and conditions of the Creative Commons Attribution-NonCommercial 4.0 International (CC BY-NC 4.0 license) (http://creativecommons.org/licenses/by-nc/4.0/).

Best quality of the inpainted image gets when the value of PSNR is high and MSE is low. Finally, the Structural Similarity Index (SSIM) is used to measure the similarity between original and inpainted images. The SSIM can be estimated using the relationship [10]:

$$SSIM(I, I') = \frac{(2\mu_I\mu_{I'}+c_1)(2\sigma_{II'}+c_2)}{(\mu_I^2+\mu_{I'}^2+c_1)(\sigma_I^2+\sigma I'^2+c_2)} \quad , \qquad 35$$

where (μ_I, σ_I) and ($\mu_{I'}$, $\sigma_{I'}$) refers to mean and standard deviation of patches in the images I and I' , respectively; $\sigma_{II'}$: the covariance of I and I'; $c_1 = (k_1 h)^2$, $c_2 = (k_2 h)^2$ such that h = $2^{bits\ per\ pixel} - 1$, k_1 = 0.01 and k_2 = 0.03. However, the value of SSIM is range from 1 to 0 and when the value is 1 means the two images are identical while 0 values refer to not identical. Thus, the qualities of inpainted images increase when the value of SSIM increases to be near 1. To test the proposed model compared with the classic model, four types of masks are selected with different images. The proposed model is used with α=1 and β=0 to recover the square missing region in case 1, the inpainted image had better restoration to the missing region with clearer edges compared with the inpainted image obtained using the isotropic model as shown in Fig. 3. In case 2, the selected missing region is chosen as a narrow horizontal rectangular line as shown in Figure 4b. Furthermore, restoration of the missing region and edges using a modified isotropic model with α=1 and β=0 enhances the treated images where the edges appeared clearer with less blurry compared with the classic model as shown in Figure 4.

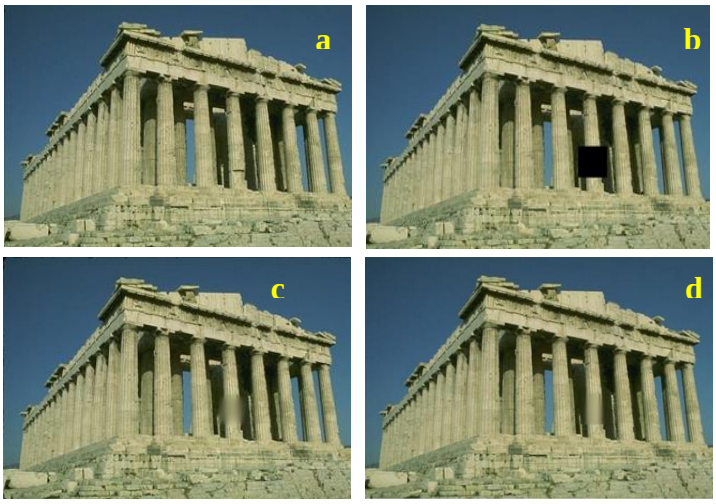

Figure3: Case1 of image inpainting (a) original image, (b) masked image, (c) and (d) inpainted image using isotropic model and proposed model, respectively.

This article is an open access article distributed under the terms and conditions of the Creative Commons Attribution-NonCommercial 4.0 International (CC BY-NC 4.0 license) (http://creativecommons.org/licenses/by-nc/4.0/).

Figure 4: Case2 of image inpainting (a) original image, (b) masked image, (c) and (d) inpainted image using isotropic model and proposed model, respectively.

In case 3, a narrow vertical rectangular missing area is selected (Figure 5b). Using the proposed model with α=0 and β=1 significantly reduced blurring and enhanced the recovery of the missing area as well as edges compared with the inpainted image obtained using the classic model as shown in Figure 5. Finally, Case 4 represents a large rectangular missing area extending horizontally on the image (Figure 6b). When using the modified isotropic model with α=1 and β=0, the blurring significantly decreased and the edges appeared partially in the painted area compared with the inpainted image obtained using the classic model as shown in Figure 6.

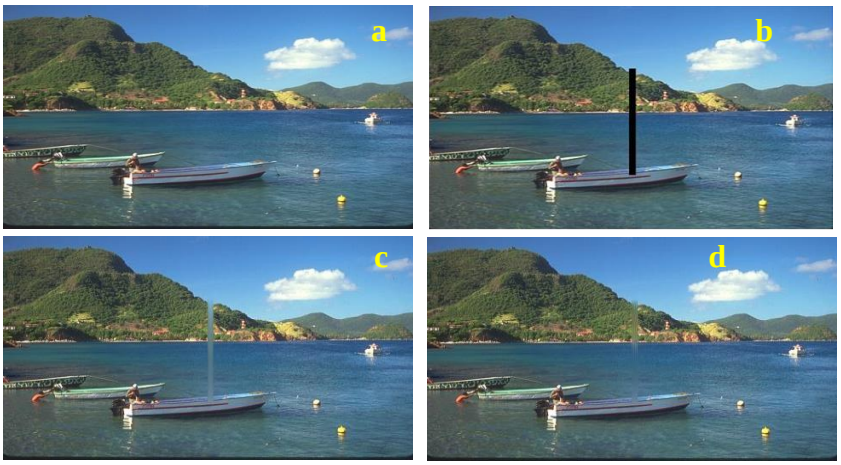

Figure 5: Case3 of image inpainting (a) original image, (b) masked image, (c) and (d) inpainted image using isotropic model and proposed model, respectively.

This article is an open access article distributed under the terms and conditions of the Creative Commons Attribution-NonCommercial 4.0 International (CC BY-NC 4.0 license) (http://creativecommons.org/licenses/by-nc/4.0/).

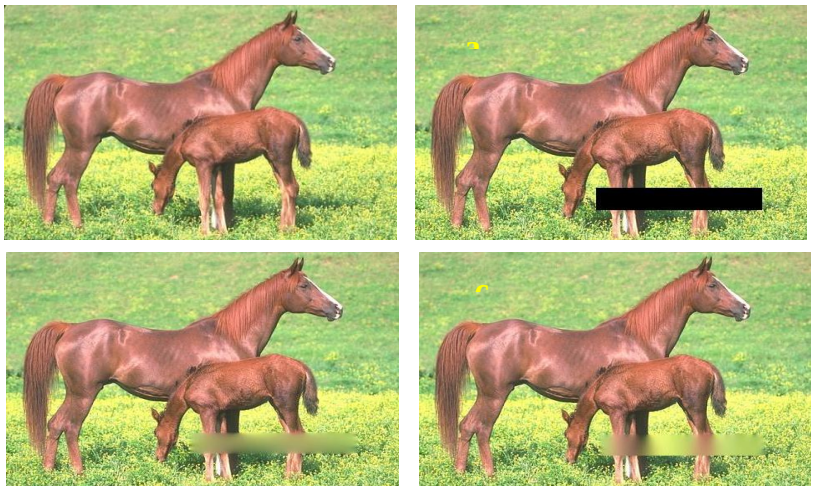

Figure 6: Case4 of image inpainting (a) original image, (b) masked image, (c) and (d) inpainted image using isotropic model and proposed model, respectively.

The MSE, PSNR, and SSIM values of these cases with different α and β values are introduced in Tables 1, 2, and 3, respectively. These tables prove the proposed model is able to fill region effectively and gives higher PSNR values with low MSE values and the SSIM values are close to 1. The proposed technique obtained higher values of SSIM and PSNR with low MSE values than the classical model as seen in Tables 1, 2, and 3, that mean the inpainted regions obtained by the proposed model are more coherent with the rest of the images for all these cases when $\alpha = 0$ and $\beta = 1$.

Table 1: MSE values or four shapes of missing region

α	β	Case1	Case2	Case3	Case4
1/2	1/2	53.287	37.922	78.462	82.636
1	0	54.691	41.318	83.914	84.261
0	1	57.180	29.361	56.330	76.184

This article is an open access article distributed under the terms and conditions of the Creative Commons Attribution-NonCommercial 4.0 International (CC BY-NC 4.0 license) (http://creativecommons.org/licenses/by-nc/4.0/).

Table 2: PSNR values for four shapes of missing region

α	β	Case1	Case2	Case3	Case4
1/2	1/2	33.3438	35.0851	29.6715	29.8571
1	0	33.4896	34.5266	30.3180	29.6170
0	1	32.6728	36.8375	31.2121	31.1774

Table 3: SSIM values for four shapes of missing region

α	β	Case1	Case2	Case3	Case4
1/2	1/2	0.477	0.657	0.334	0.393
1	0	0.458	0.636	0.328	0.410
0	1	0.484	0.641	0.475	0.362

Table 4 summarizes the values of MSE, PSNR, and SSIM obtained from images that were inpainted using the classic isotropic model and proposed model with different values of α and β. The image quality confirmed that the proposed model is outperforming the classical model. The proposed model is effective and capable to fill the missing region and gives higher PSNR value with a low MSE. The measurements confirmed that the value of SSIM value increased when the proposed model was compared to the original model which means the inpainted seems more similar to the original ones. Further, there is also a very clear and significant improvement in time.

This article is an open access article distributed under the terms and conditions of the Creative Commons Attribution-NonCommercial 4.0 International (CC BY-NC 4.0 license) (http://creativecommons.org/licenses/by-nc/4.0/).

Table 4: Image inpainted quality assessment comparison using MSE, PSNR, and SSIM.

Cases	Model	MSE	PSNR	SSIM	Time (S)
Case1	Isotropic	22.85881	34.68158	0.63376	39.8294
	Modified isotropic	11.43862	38.21239	0.60564	1.88148
Case2	Isotropic	23.88252	34.38542	0.88483	2.77682
	Modified isotropic	12.20463	37.30076	0.93475	0.68811
Case3	Isotropic	30.92779	33.48105	0.78239	111.222
	Modified isotropic	22.01346	35.07477	0.80704	13.9987
Case4	Isotropic	72.54162	30.23256	0.47157	389.569
	Modified isotropic	47.29332	34.22688	0.46518	8.9966

5. Conclusions

The modified isotropic model gives good results if the missing areas are small, but the repainting efficiency of the equation is lower. If the areas are large in applying the properties equation, then all the results are blurry, while the modified model succeeded in partially restoring the edges and providing more clarity and reducing the blurring in the missing area and succeeded in showing more details than in the case of using the classic isotropic model, the modified model succeeds when The direction of texture stretching out of the region is in the direction of diffusion of the additive derivative and the result improves as the surrounding area of missing area is less texture. This is what the statistical results showed by MSE, SSIM ,PSNR quality measurement .

This article is an open access article distributed under the terms and conditions of the Creative Commons Attribution-NonCommercial 4.0 International (CC BY-NC 4.0 license) (http://creativecommons.org/licenses/by-nc/4.0/).

References

[1] Z. Qin, Q. Zeng, Y. Zong, F. Xu, Image inpainting based on deep learning: A review, Displays 69 (2021) 102028, https://doi.org/10.1016/j.displa.2021.102028

[2] F. Berntsson, G. Baravdish, Coefficient identification in PDEs applied to image inpainting, Appl Math. Comput., 242(2014)227-235, https://doi.org/10.1016/j.amc.2014.05.051

[3] A.K Al-Jaberi, A. Asaad, S.A Jassim, N.Al-Jawad, Topological Data Analysis for Image Forgery Detection., Indian J. Forensic Med. Toxicol., 14(2020)1745-1751 https://doi.org/10.37506/ijfmt.v14i3.10668

[4] A.K. Al-Jaberi, E.M. Hameed, Topological Data Analysis For Evaluating PDE-based Denoising Models, J. Phys.: Conf. Ser., 1897 (2021) 012006, https://doi.org/10.1088/1742-6596/1897/1/012006

[5] A. Theljani, Z. Belhachmi, M. Moakher, High-order anisotropic diffusion operators in spaces of variable exponents and application to image inpainting and restoration problems, Nonlinear Analysis: Real World Appl., 47(2019) 251-271, https://doi.org/10.1016/j.nonrwa.2018.10.013.

[6] X. Zhu, Y. Qian, X. Zhao, B. Sun, Y. Sun, A deep learning approach to patch-based image inpainting forensics, Signal Processing: Image Commun., 67(2018)90-99, https://doi.org/10.1016/j.image.2018.05.015

[7] T. Xu, T.Z. Huang, L.J. Deng, X.L. Zhao, J.F. Hu, Exemplar-based image inpainting using adaptive two-stage structure-tensor based priority function and nonlocal filtering, Journal of Visual Communication and Image Representation, 83(2022)103430, https://doi.org/10.1016/j.jvcir.2021.103430

[8] S. Masnou, J.-M. Morel, Level lines based disocclusion, in Proceedings 1998 International Conference on Image Processing. ICIP98, 3(1998)259–263, http://dx.doi.org/10.1109/ICIP.1998.999016.

[9] M. Bertalmio, G. Sapiro, V. Caselles, C. Ballester, Image inpainting, in In Proc. ACM Conf. Comput. Graph., (2000) 417–424.

[10] A Halim, B.V. Rathish Kumar, An anisotropic PDE model for image inpainting, Comp. Math. Appl., 79(2020)2701-2721, https://doi.org/10.1016/j.camwa.2019.12.002

This article is an open access article distributed under the terms and conditions of the Creative Commons Attribution-NonCommercial 4.0 International (CC BY-NC 4.0 license) (http://creativecommons.org/licenses/by-nc/4.0/).

[11] S.H. Saleh, S.A. Haddad, Effect of anisotropic permeability on double-diffusive bidisperse porous medium, Heat Transf., 49(2022) 1825-1841, https://doi.org/10.1002/htj.21695

[12] S. Haddad, Thermal Convection in a Rotating Anisotropic Fluid Saturated Darcy Porous Medium, Fluids, 2(2017) 44, https://doi.org/10.3390/fluids2030044

[13] A Theljani, Z Belhachmi, M Moakher, High-order anisotropic diffusion operators in spaces of variable exponents and application to image inpainting and restoration problems, Nonlinear Analysis: Real World Appl., 47(2019) 251-271, https://doi.org/10.1016/j.nonrwa.2018.10.013

[14] A.K. Al-Jaberi, A. Asaad, S.A. Jassim, N. Al-Jawad, Topological data analysis to improve exemplar-based inpainting", Proc. SPIE 10668, Mobile Multimedia/Image Processing, Security, and Applications 2018, 1066805, https://doi.org/10.1117/12.2309931

[15] Z. Wang, A.C Bovik, H. R. Sheikh, E.P. Simoncelli, Image Quality Assessment: From Error Visibility to Structural Similarity, IEEE Transactions On Image Processing, 13(2004)1-14

[16] K.R. Patel, L. Jain, A.G. Patel, Image inpainting, a review of the underlying different algorithms and comparative study of the inpainting techniques, Int. J Comp. Appl., 118(2015)32-38, DOI:10.5120/20784-3422

[17] Gi Aubert, P Kornprobst, Mathematical Problems in Image processing Partial Differential Equations and the Calculus of Variations, 2nd edition, Springer, 2006.

[18] C Guillemot, O L Meur, Image Inpainting: Overview and Recent Advances, IEEE Signal Processing Magazine, 31(2014)127-144, DOI: 10.1109/MSP.2013.2273004

[19] A k Aljaberi, E M. Hameed, A review of PDE-based local inpainting methods, J Phys.: Conference Series 1818 (2021) 012149, doi:10.1088/1742-6596/1818/1/012149

[20] M.N. Özisik¸ H.R.B. Orlande, M.J. Colaço, R.M. Cotta, Finite Difference Methods in Heat Transfer, 2ed, Taylor & Francis Group, LLC, USA, 2017.

[21] The Berkeley Segmentation Dataset and Benchmark, 2007, https://www2.eecs.berkeley.edu/Research/Projects/CS/vision/bsds/

This article is an open access article distributed under the terms and conditions of the Creative Commons Attribution-NonCommercial 4.0 International (CC BY-NC 4.0 license) (http://creativecommons.org/licenses/by-nc/4.0/).

تقنية جديدة للطلاء الداخلي للصور تعتمد على انتشار الخواص

زينب علي عبد الكريم[1] و احمد كاظم الجابري[2]

1 قسم الرياضيات ، كلية العلوم ، جامعة البصرة ، البصرة ، العراق

2 قسم الرياضيات ، كلية التربية للعلوم الصرفة ، جامعة البصرة ، البصرة ، العراق.

المستخلص

تم اقتراح تقنية جديدة معتمدة على نموذج الانتشار isotropic model لاستعادة المناطق المفقودة في الصورة الرقمية تعتمد هذه التقنية على تعديل نموذج الانتشار الكلاسيكي .classical isotropic model وتم تطبيقه على الصور الطبيعية لاستعادة المناطق المفقودة المختلفة في الشكل والمساحة وتمت مقارنة نتائج النموذج المعدل مع النموذج الكلاسيكي التي تم الحصول عليها وتبين تفوق النموذج المعدل على النموذج الكلاسيكي من حيث بناء النسيج في المنطقة المفقودة واستعادة المناطق الكبيرة تم استخدام العديد من مقاييس الجودة لحساب فعالية النموذج المقترح مثل MSEو PSNRو SSIM يظهر النموذج المعدل معايير جودة افضل لعدد كبير من الصور الطبيعية مع أداء افضل مقارنة بنموذج الانتشار الكلاسيكي

This article is an open access article distributed under the terms and conditions of the Creative Commons Attribution-NonCommercial 4.0 International (CC BY-NC 4.0 license) (http://creativecommons.org/licenses/by-nc/4.0/).